Available online at www.sciencedirect.com

SciVerse ScienceDirect

journal homepage: www.elsevier.com/locate/he

Mesoporous carbon supported nanoparticulated $PdNi_2$: A methanol tolerant oxygen reduction electrocatalyst

Guadalupe Ramos-Sánchez [a], *Mariano M. Bruno* [b,c], *Yohann R.J. Thomas* [b], *Horacio R. Corti* [b], *Omar Solorza-Feria* [a,*]

[a] *Departamento de Química, Centro de Investigación y Estudios Avanzados del IPN, Av. IPN 2508, Col. San Pedro Zacatenco, A. Postal 14-740, 07360 México D.F., Mexico*

[b] *Departamento de Física de la Materia Condensada, Comisión Nacional de Energía Atómica, Av. Gral. Paz 1499, C.P. 1650, San Martín, Buenos Aires, Argentina*

[c] *Escuela de Ciencia y Tecnología, Universidad de Gral. San Martín, Martin de Irigoyen 3100 (1650), San Martín, Buenos Aires, Argentina*

ARTICLE INFO

Article history:
Received 23 June 2011
Received in revised form
25 August 2011
Accepted 27 August 2011
Available online 19 October 2011

Keywords:
Carbon
Mesoporous
Support
$PdNi_2$
Nanocatalyst
Oxygen reduction reaction

ABSTRACT

The kinetics of the oxygen reduction reaction (ORR) of $PdNi_2$ nanoparticles supported on a high specific area mesoporous carbon (MC) and Vulcan carbon was studied in the presence and absence of methanol in acid media. The electrocatalysts, synthesized by chemical reduction of the metal chlorides with $NaBH_4$ in aqueous media were characterized by X-ray diffraction (XRD) and transmission electron microscopy (TEM). The catalyst supported on MC has a higher degree of Ni alloying and a smaller particle size than that supported on Vulcan. The electrochemical characterizations by RDE and DEMS indicate that $PdNi_2$ supported on the high surface area MC exhibits higher catalytic activity for the ORR, very similar to that of Pd- and Pt-based alloys with the advantage of a very low noble metal loading. Moreover, the $PdNi_2$ supported on MC shows an excellent methanol tolerance in acid media. Thus, this novel combination catalyst/support would be a suitable cathodic catalyst for direct methanol fuel cells.

1. Introduction

Electrocatalysts nanotechnology is an emerging area of interest, which opens up new possibilities of applications of novel materials for the renewable energy sector. Most of the research in advanced electrocatalysts is performed on powders containing nanometric-sized particles [1–4]. Because the fuel cell efficiency is related to the catalyst activity, *i.e.*, the size, geometry, composition, dispersion of its particles and interaction with the support, it remains important the control of these factors during the synthesis process.

In the renewable energy sector Direct Methanol Fuel Cells (DMFC) is also an attractive fuel cell due to the advantage of the use of a liquid fuel [5]. However, the permeation of alcohol through the membrane (crossover phenomenon) produces a loss of efficiency and a decrease of the fuel cell voltage due to parasitic methanol oxidation at the cathode, which remain as one of the major problems for the performance of the DMFC [6,7].

One of the critical issue to be addressed in fuel cells is the lack of effective cathodic electrocatalysts for the multi-electron charge transfer processes of oxygen reduction

* *Corresponding author*. Tel.: +52 55 5747 3715; fax: +52 55 5747 3389.
E-mail address: osolorza@cinvestav.mx (O. Solorza-Feria).

0360-3199/$ – see front matter Copyright © 2011, Hydrogen Energy Publications, LLC. Published by Elsevier Ltd. All rights reserved.
doi:10.1016/j.ijhydene.2011.08.113

reaction (ORR) at low overpotential. Platinum-based electrocatalysts are usually employed for the cathode reaction in PEMFC and DMFC, although its high cost and limited resources encouraged the study of alternative metals. Pure palladium is less expensive than Pt but its electrocatalytic activities for ORR is at least five times lower than of Pt. For this reason, great efforts have been devoted to improve the electroactivity of Pd by alloying with transition metals [8,9].

The anion poisoning of Pd in alkaline solutions is lower than in acid media, leading to a higher ORR activity in alkaline media, comparable to that of Pt [10]. Pd alloys with Fe [10], Sn [11], and Au [12] are more active than pure Pd in alkaline solutions. Ni alloys having compositions PdNi and Pd_3Ni exhibited the highest ORR activities, although they were not superior to that of pure Pd and Pt [13].

There are several studies of the ORR activities of Pd alloys in acidic solutions [8]. Savadogo and coworkers observed for the first time the enhanced ORR activities on sputtered Pd alloys with Co, Ni and Cr, and more recently Pd–Cu alloys [14,15]. The system Pd–Co has been extensively studied [16–18] and the optimal composition seem to be close to Pd_2Co, while for the Pd–Fe systems the Pd_3Fe catalyst has ORR activities comparable to or higher than that of Pt and Pd_2Co. Di Noto et al. [19] reported Pd–Co catalysts supported on carbon-nitride with ORR activities higher than that of Pt. Pd–Cu [15,20], Pd–Ti [21], and Pd–Ni [22] binary system have also been studied in acidic media.

The ORR activities of Pd ternary systems in acidic media have been also reviewed by Shao [8]. Ramos-Sanchez and Solorza-Feria [23] have reported that Pd and bimetallic chalcogenide alloys dispersed in Vulcan exhibit better catalytic activity than Pd alone.

Several carbon supported nanoparticles of Pd and its alloys have been reported to exhibit significant ORR activity in presence of methanol [8,9,15,22]. The higher methanol tolerance of the Pd-M alloys over Pt in acid media, including Pd–Co, Pd–Fe, Pd–Cr, Pd–Ni, and Pd–Pt [16,24,25] catalysts, encourages their use as cathodic electrocatalysts in alcohol direct fuel cells. Paradoxically, several works have reported the use of Pd–Ni catalysts for the oxidation of alcohols in alkaline fuel cells [26–29].

As quoted by Shao [8], the interaction between the support and metal nanoparticles and its effect on the ORR activity is a topic that has not been studied deeply. New types of novel nanostructured carbon have been investigated as electrocatalysts support such as carbon nanotubes [30], fibers of carbon [31], carbon silica composite [32] and mesoporous carbon [33–35].

The Vulcan XC-72 carbon black has been the most used carbon support in fuel cells [36]. However, the blocking of the oxygen transportation reduces the reactive sites to obtain high current densities when carbon black is used as electrocatalyst support. This behavior is also attributed to elevated quantity of water transported by diffusion and electro-osmotic pressure from the anode through the Nafion® membrane [37]. For this reason, mesoporous carbon has been taken into consideration as electrocatalyst support on the last years [38], because it exhibits good structural properties such as high catalyst dispersion, very interconnected pores for easy diffusion and transportation of reactants and sub-products, beside its high electrical conductance which are attractive for fuel cells application [39,40].

The purpose of this work is to study the kinetics of the ORR on a nanoparticulated $PdNi_2$ ink-type electrode in 0.5 M H_2SO_4. The catalytic activity was determined for the catalyst supported on a new mesoporous carbon and Vulcan XC-72 carbon black, both with $PdNi_2$ catalyst loading of 45 wt.%. The combination of the nanoparticulated $PdNi_2$ catalyst and the high specific area mesoporous carbon support constitutes a completely new approach in the search of more efficient cathode catalyst in direct methanol PEM fuel cells, where the crossover of methanol severely reduces the efficiency of the membrane-electrode assembly.

2. Experimental

2.1. Carbon preparation and characterization

The mesoporous carbon (MC) support was prepared using the method described elsewhere [41]. Briefly, a precursor was prepared by polymerization of resorcinol (Fluka) and formaldehyde (Cicarelli, 37 wt. %). Sodium acetate (Cicarelli) was used as catalyst and the cationic polyelectrolyte polydilayldimethylammonium chloride (PDADMAC, Sigma–Aldrich) as structuring agent. The reactive mixture of resorcinol (R), formaldehyde (F) and sodium acetate (C) was stirred at 40 °C for 10 min before the addition of PDADMAC (P). The molar ratio of the components R:F:C:P was 1: 3: 0.04: 0.03.

Once the mixture became homogenous, the solution was heated to 70 °C for 48 h at atmospheric pressure. The resulting brown monolithic RF polymer piece was dried in air for 3 days. The polymer was then carbonized under nitrogen stream in a tubular furnace by heating the sample, from ambient temperature to 1000 °C, at a rate of 40 °C per hour. Finally the resulting material was grinded and passed through a mesh with a pore size of 40 μm.

An ASAP 2020 (Micrometrics) instrument was used to determine the nitrogen adsorption isotherms at −196 °C for calculating the total volume of micropores through the Dubinin-Radushkevitch (DR) equation [42], and the specific surface area through the Brunauer–Emmett–Teller (BET) equation [43].

Vulcan XC-72 carbon (VC) with a BET surface area of 220 $m^2\ g^{-1}$ from Cabot Corporation was used as an alternative support. This non-porous carbonous material, having particle sizes of 40–50 nm, is the carbon support usually employed for anodes and cathodes of PEM fuel cells feed with hydrogen or methanol. The chemical composition of the bimetallic catalyst was determined using an Energy Dispersive X-Ray Spectroscopy, EDX (Falcon PB8200), coupled to a SEM (Philips, model 515).

2.2. Electrocatalyst synthesis and characterization

$PdNi_2$ nanocatalyst was synthesized by borohydride chemical reduction of $PdCl_2$ (Sigma–Aldrich 99%) and $NiCl_2 \cdot 6H_2O$ (Sigma–Aldrich 99.9999%) with a molar ratio 1:2 in aqueous media. The precursors were dissolved in 200 ml of distilled water and the amount of carbon support required to obtain a metal loading of 45 wt. % was added, maintaining a vigorous agitation of the solution for 30 min. A three-fold excess of $NaBH_4$ (Sigma–Aldrich >98.5%) was added as a reducing agent

and the reaction product was washed several times to remove the sodium chloride byproduct. The filtered powder was dried at 70 °C under vacuum and used for physical and electrochemical characterizations. The catalysts prepared on mesoporous and Vulcan carbon are denominated $PdNi_2$/MC and $PdNi_2$/VC, respectively. The molar ratio Pd:Ni was chosen according to a previous analysis in which the catalytic activity of $PdNi_2$ was similar to that of PdNi [44], while maintaining the stability of the catalyst. Electrochemical characterization of PdNi/CV samples prepared by the chemical methodology reported previously [23,44], with Pd:Ni 2:1, 1:1 and 1:2 M ratios is included in the supplementary information. There in, very similar current-potential behaviors despite the different proportion of precursors in the synthesis was observed. Therefore, the $PdNi_2$ catalyst was selected for the electrocatalytic study because it contains a lesser quantity of the noble metal, which implies a reduced cost of the nanocatalyst.

Powder X-ray diffractograms of the $PdNi_2$/MC and $PdNi_2$/VC electrocatalysts were performed on a Diffrac Brucker AXS, D8 Advanced Plus diffractometer using a monochromatic CuKα radiation ($\lambda = 0.154056$ nm) and operating at 35 kV and 30 mA. A 2θ scanning range from 30° to 90° was explored at a step scan rate of 0.02° every 15 s. XRD data were analyzed with Topas Academic software to identify the XRD patterns and to perform the Rietveld analysis.

2.3. Electrochemical set-up and electrode preparation

Electrochemical experiments were performed in a three-electrode cell. Cell temperature was controlled by a Haake thermostat (model DC1) at 25 °C. A platinum mesh was used as the counter electrode, and Hg/Hg_2SO_4/0.5 M H_2SO_4 (0.680 V *vs.* NHE) as reference electrode. A 0.5 M H_2SO_4 solution prepared from double distilled water and sulfuric acid (Aldrich) was used as electrolyte.

The determination of electrochemical active surface area (EAS) was performed by cyclic voltammetry in nitrogen saturated acid solution, in conjunction with CO striping. The electrode potential was held at 0.25 V/NHE and CO (UHP grade) bubbled for 1 h. Thereafter, the CO was removed by purging the electrolyte with nitrogen for 15 min and the test electrode swept from 0.05 V to 1.25 V/NHE at 3 mV s^{-1}.

Rotating disk electrode (RDE) measurements were conducted on a potentiostat/galvanostat (PARSTAT model 2273). The ink-type working disk electrode was prepared by depositing the catalyst ink onto the surface of a glassy carbon electrode (0.07 cm^2) mounted in an interchangeable holder (Pine Instruments). The catalyst ink was prepared by mixing 2 mg $PdNi_2$/MC or $PdNi_2$/VC with 6 μL of 5 wt. % Nafion (DuPont, 1100 EW) and 60 μL of isopropyl alcohol. The resulting suspension was sonicated for 5 min and 2 μL of the ink was deposited onto the glassy carbon electrode surface for the RDE experiments. The estimated amount of catalyst loading on the electrode surface was about 0.86 mg cm^{-2}.

2.4. DEMS set-up and cell

The DEMS setup consists of two differentially pumped chambers and a quadrupole mass spectrometer (Pfeiffer, EVN 116). The electrochemical cell was connected to a primary vacuum chamber pumped with a rotary vane pump (DUO 5 Pfeiffer), and a liquid nitrogen cold trap was included in this section to avoid the inleakage of oil vapours. The secondary chamber was evacuated at 60 L s^{-1} by a turbomolecular pump backed by a dry diaphragm Pfeiffer turbo drag pumping station (TSH/U 071 E). A gas-dosing valve (Pfiffer, EVN 116) connects the two chambers. The quadrupole mass spectrometer was connected to the secondary chamber and contains a continuous dynode secondary electron multiplier/Faraday cup detector with a sensitivity of 200 $Ambar^{-1}$ (QMS 200 M1, Prisma™).

A stationary flow electrochemical cell, similar to that used by Planes et al [45], was located on the top of the DEMS intake, on the primary vacuum chamber. The working electrode was a glassy carbon electrode of 6 mm diameter with a hole of 0.8 mm diameter in the electrode center.

A porous Teflon® membrane separates the cell from the DEMS intake, and allows the flow of the volatile products of the electrochemical reaction toward the analysis chamber. The working electrode and the cell were designed in such a way that the electrode was separated *ca.* 150 μm from the porous membrane, while the solution in this thin layer was in contact with the bulk solution in the cell. Cyclic voltammograms were performed with an Autolab potentiostat (PGSTAT302N), while the volatile reaction products were monitored by the mass spectrometer.

The ink-type working disk electrode was prepared by depositing uL of the catalyst ink (described above) onto the surface of a glassy carbon electrode (1.13 cm^2). $PdNi_2$/MC, $PdNi_2$/VC catalysts and Pt supported on Vulcan carbon (E-TEK) used for comparison, were analyzed using DEMS technique. The ink formulation and electrode area lead to a catalyst loading of 0.24 mg cm^{-2} for DEMS experiments.

3. Results and discussion

3.1. Carbon characterization

The nitrogen adsorption-desorption isotherms and pore size distribution of carbonized material at 1000 °C are shown in Fig. 1. The analysis of the mesoporous carbon using the DR equation indicates the presence of pores having sizes smaller than 2 nm. The total pore volume (at $p/p^\circ = 0.986$) is 0.99 cm^3 g^{-1} and the micropore volume deduced by DR was 0.23 cm^3 g^{-1}. A maximum in the pore size distribution is found at around 20 nm. The micro- (<2 nm) and meso-porosity (between 2 and 50 nm) is attributed to the structure of the carbon, which consists of clusters of porous uniform spheres in a fairly regular array [41]. The BET equation yields to a high specific surface area (580 m^2 g^{-1}) and the hysteresis loop at high relative pressure is associated to the mesoporous materials.

3.2. Catalyst characterization

Fig. 2 shows the XRD patterns of $PdNi_2$ catalysts supported on mesoporous and Vulcan carbon. The five characteristic diffraction peaks resembles reflections of the face-centered cubic (fcc) crystal lattice of the Pd (JCPDS card code 65-6174),

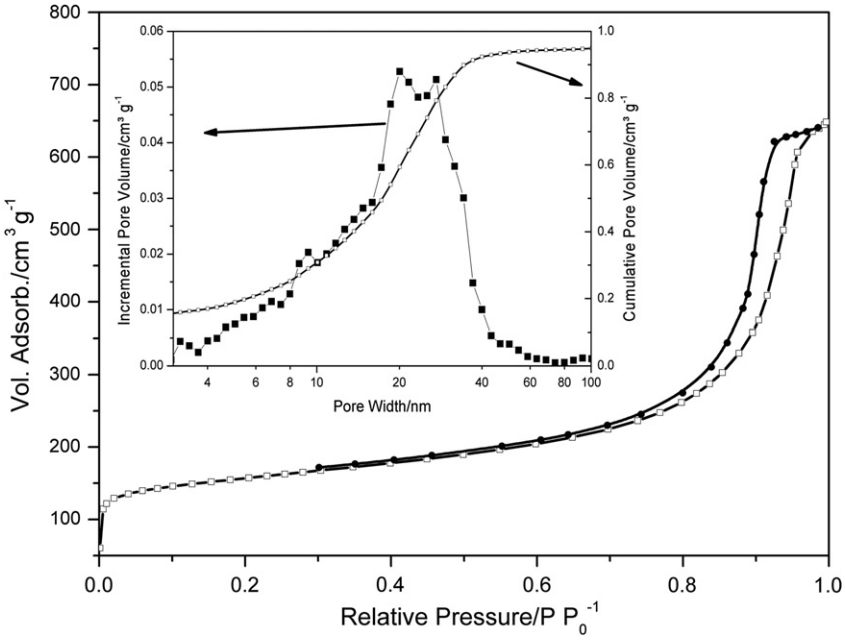

Fig. 1 – Nitrogen adsorption-desorption isotherms. Inset: pore size distribution.

while the peak at 60° correspond to Ni hcp [46], and the small peak at 33° is probably due to $Ni(OH)_2$ phase (JCPDS 14–0117). Rietveld analysis of the samples revealed the presence of a Ni rich phase in $PdNi_2$/VC while in $PdNi_2$/MC a minimal quantity of Ni rich phase is detected (Table 1). The diffraction peaks in the $PdNi_2$ catalyst are slightly shifted to higher 2θ values (see inset of Fig. 2) with respect to the corresponding peaks in the Pd catalyst, this shift in peaks position can be associated to the alloy formation because partial substitution of Pd by Ni in the fcc structure produces a contraction of the lattice.

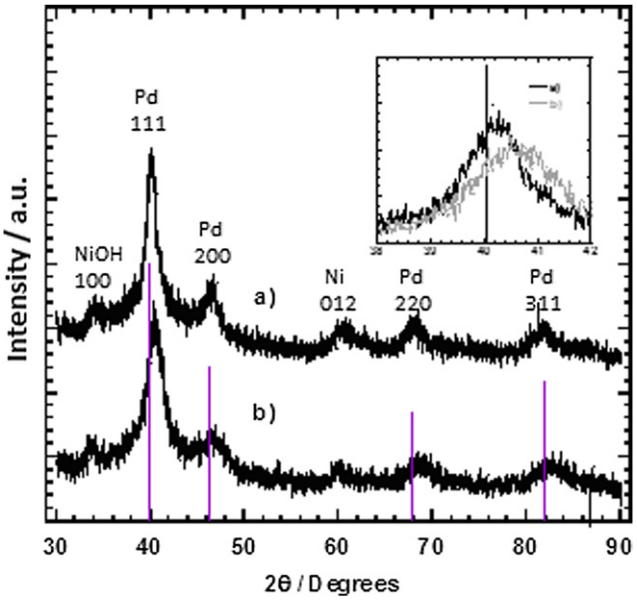

Fig. 2 – XRD patterns of $PdNi_2$ catalysts on different supports: (a) $PdNi_2$/VC and (b) $PdNi_2$/MC. The lines indicate the Pd (fcc) peaks. Inset: zoom of the peaks at 2θ ≈ 40°.

The lattice parameter was calculated from XRD data [47] and equation (1), being λ the wavelength of the X-ray source and θ the position of diffraction peak.

$$a = \frac{\sqrt{2}\lambda}{\sin\theta} \quad (1)$$

According to Vergard's law there is a linear dependence of the lattice parameter with the Ni content, which is:

$$x_{(Ni)} = \frac{a - a_0}{a_{alloy} - a_0} \quad (2)$$

where a is the lattice parameter of the PdNi catalyst that depends on composition, a_{alloy} is the lattice parameter for a PdNi solid solution [48,49] and a_0 is the lattice parameter of Pd. The analysis was done over the Pd (200) peak, indicating that there is higher quantity of Ni alloyed in the $PdNi_2$/MC than in $PdNi_2$/VC. Table 1 summarize results of lattice parameters, Ni alloyed, Rietveld analysis and chemical composition by EDX.

The broad peaks at the low angle scattering region suggests the presence of nanocrystallites. The size of the crystallites, determined with the Topas Academic Software, were 5 nm for $PdNi_2$/MC and 7 nm for $PdNi_2$/VC catalysts. The TEM images of synthesized $PdNi_2$ samples are shown in Fig. 3, where well distributed particles, with a nearly uniform size, are observed. EDX results confirm that 1:2 ratio of Pd:Ni composition is almost maintained in good agreement with its estimated stoichiometry.

3.3. *Electrochemical characterization*

Cyclic voltammetry was used for determination of the EAS with the CO adsorption and stripping. The CO stripping electro-oxidation with the corresponding post-oxidation

Table 1 – XRD and EDX analysis of supported $PdNi_2$ samples.

	Pd:Ni EDX	Lattice parameter/Å	x_{Ni} Alloyed	Rietveld analysis % phase		
				Pd fcc	Ni hcp	$Ni(OH)_2$
$PdNi_2$/VC	37:63	3.856	0.28	68	24	8
$PdNi_2$/MC	33:68	3.874	0.58	89	0.5	10.5

voltammogram (not included) was taken as a reference base line. The EAS was calculated by using equation (3):

$$EAS = \frac{Q}{m_c Q_{Pd,CO}} \quad (3)$$

where $Q_{Pd,CO} = 0.42$ mC cm^{-2} [50] is the charge associated with the formation of a CO monolayer in the test electrode surface, m_c is the catalyst load, and Q the integrated area under the CO desorption peak. Values of 17.3 m^2 g^{-1} and 18.8 m^2 g^{-1} for PdNi/VC and PdNi/MC, respectively, were calculated from measured charges. These results indicate a better dispersion of the catalyst on the mesoporous carbon.

Fig. 4 shows the steady-state current-potential curves for the ORR on $PdNi_2$ supported on mesoporous (Fig. 4a) and Vulcan carbon (Fig. 4b). The polarization curves were recorded in cathodic direction starting from the open circuit potential (0.92 V *vs.* NHE) up to 0.3 V *vs.* NHE, and rotation speed in the range of 200–1600 rpm. The dependence of the cathodic current with the potential and rotation speed is observed in both figures. The electrochemical reaction seems to be under kinetic and mixed activation-diffusion control in all the

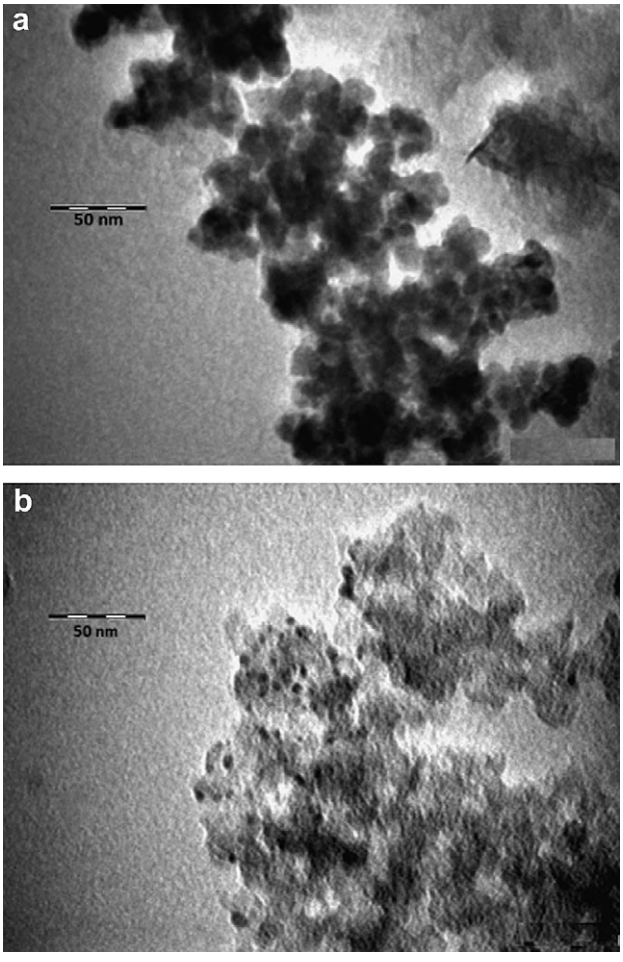

Fig. 3 – TEM micrographs of the as synthesized catalysts. a) $PdNi_2$/VC and b) $PdNi_2$/MC.

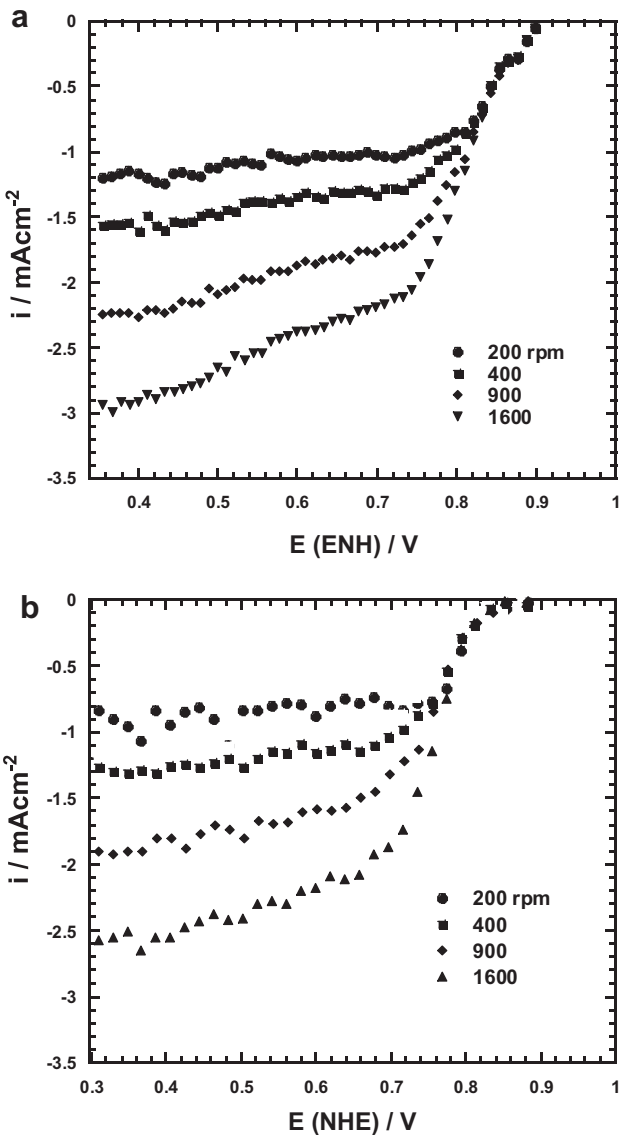

Fig. 4 – Steady-state current-potential curves for ORR on $PdNi_2$ supported on (a) MC and (b) VC at different rotation rates, in an oxygen-saturated 0.5 M H_2SO_4 electrolyte.

potential range. Current increased with increases rotation speed due to the enhanced oxygen diffusion toward the electrode surface. The experimental average slope value agrees with the theoretical slope of the Koutecky–Levich equation (3), calculated taking into consideration reported parameters [50,51], suggesting that the ORR proceed toward water formation via the overall four-electron transfer reaction (*i.e.*, $O_2 + 4H^+ + 4e^- \rightarrow 2H_2O$).

Fig. 5 shows the mass-transfer corrected Tafel plot for the $PdNi_2$ catalyst supported on mesoporous and Vulcan carbon and the corresponding kinetic current, i_k, determined by Eq. (4) [52]:

$$i_k = \frac{i_L i}{i_L - i} \tag{4}$$

with the limiting current, i_L:

$$i_L = 0.62nFAD^{2/3}\omega^{1/2}\nu^{-1/6}C \tag{5}$$

i being the measured current. The limiting currents were obtained from the Koutecky–Levitch plot (1/i vs $\omega^{-1/2}$), following the procedure described in literature [50,51,53].

The kinetic parameters reported in Table 2, indicate that in both carbon supports, MC and VC, the catalytic activity of the $PdNi_2$ catalyst for the ORR is within the order of magnitude reported for bimetallic catalysts and it is acceptable for use as cathode electrodes in fuel cells. The Tafel slope is close to 60mV/dec in both supported catalyst. However, it should be noted the lower overpotential required to reach the same current density in the catalyst supported on mesoporous carbon. In summary, the kinetic parameters for $PdNi_2$/MC show that this catalyst is able to drive the ORR at very similar rate compared to Pd- nad Pt- based alloys reported in the literature as the state of art (see Table 2), with the advantage of a very low noble metal loading [1,54–56]. This is attributed to a better distribution of $PdNi_2$ catalyst on the mesoporous support and to the higher amount of Ni alloyed in the $PdNi_2$/MC in relation to Ni alloyed in $PdNi_2$/VC.

Table 2 – Kinetic parameters of $PdNi_2$ catalyst on VC and MC and other catalyst reported in the literature.

	−b (mV dec^{-1})	i_0 (mA cm^{-2})	E @ 1 mA cm^{-2} (V)	Ref.
$PdNi_2$/VC	65	2.94 E−08	0.796	thiswork
$PdNi_2$/MC	62	5.78 E−07	0.769	thiswork
Pt/C	52	1.33E−06	–	[54]
Pt–Cu/C	48	4.33 E−08	–	[54]
Pd–Cu	98	5.8 E−06	–	[1]
Pd-Cu- 500 °C	–	–	~0.8	[55]
PdNi/C	60	–	~0.73	[56]
Pt–PdNi/C	60	–	~0.81	[56]

3.4. DEMS characterization

It has been demonstrated that some palladium-based catalysts exhibit high tolerance to methanol oxidation reaction (MOR) and are stable in the presence of methanol [22,57,58]. In order to analyze the electro-oxidation of methanol on the supported $PdNi_2$ catalysts, and compare with Pt/C catalyst (20 wt. %, E-TEK), we performed DEMS characterization on these materials in O_2 saturated 0.5 M CH_3OH + 0.5 M H_2SO_4 solution.

Some of the volatile products and secondary product species can be monitored online by DEMS during methanol oxidation. In Fig. 6 the electrochemical current, and the ionic current of mass spectrometric (I_{ms}) for carbon dioxide ($m/z = 44$) and metylformiate ($m/z = 60$) formation on the Pt/VC catalyst are shown. Methylformiate detection indicates the formation of formic acid as a side product. Behm and coworkers studied in detail the DEMS behavior of Pt/C electrodes under similar conditions [59–62]. Their conclusions can be briefly summarized as follows: i) the methanol electro-

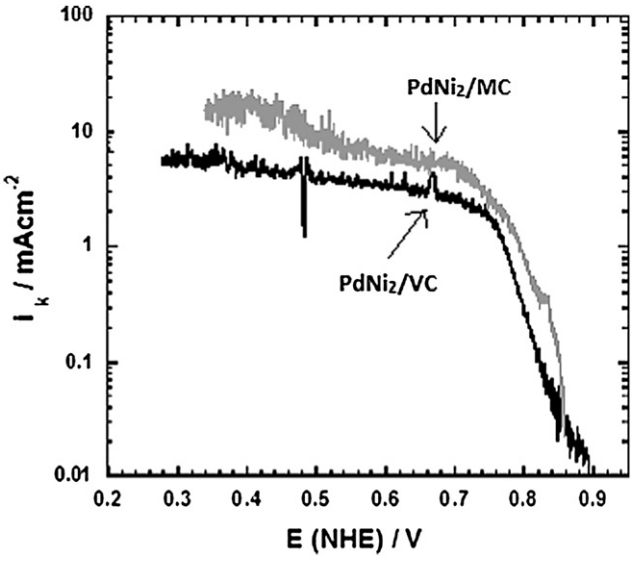

Fig. 5 – Mass-transfer corrected Tafel plots for $PdNi_2$ electrocatalysts supported on MC and VC.

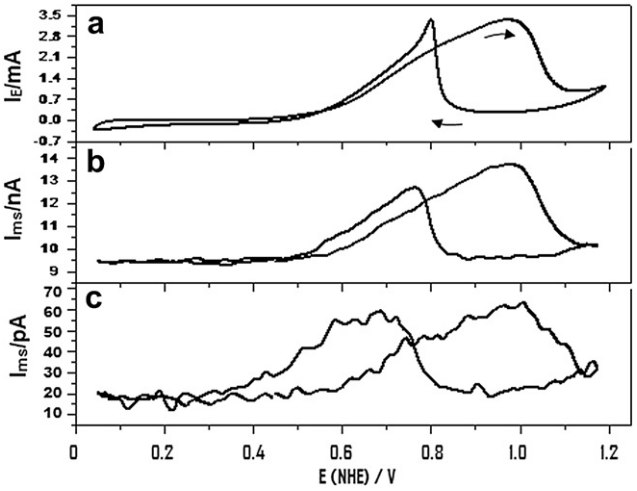

Fig. 6 – Cyclic voltammetry and potentiodynamic DEMS ionic currents of Pt/VC in O_2 saturated 0.5 M H_2SO_4 + 0.5 M methanol. a) electrochemical current (arrows indicate sweep direction); b) ionic current corresponding to $m/z = 44$ (CO_2); and c) $m/z = 60$ (methylformiate).

oxidation produces CO-type species that adsorbed on the platinum active sites blocking them; ii) hydroxyl species created by water dissociation is necessary for removal adsorbed species; iii) at higher positive potentials the MOR is inhibited by PtO formation at the electrode surface; iv) in the reverse scan the MOR is reactivated together with the reduction of PtO; v) the subsequent decay in the current is due to re-poisoning of the catalyst surface by adsorbed methanol dehydrogenation residues; vi) the shape of the ion current curves follows that of the faradaic current.

Similar DEMS characterizations were performed for $PdNi_2$/VC and $PdNi_2$/MC catalysts. Fig. 7(a–e) and Fig. 7(f–j) show the current-potential responses in acid media for $PdNi_2$/VC and $PdNi_2$/MC, respectively. Fig. 7a (VC) and 7f (MC) shows the electrochemical response of both catalyst in H_2SO_4 (nitrogen saturated) which is similar to Pd catalyst [53]. The peak of the oxide reduction is shifted to more anodic potential in relation to that reported for pure Pd, indicating that the incorporation of Ni in the Pd structure inhibits the chemisorption of OH^- ions on the Pd sites [22,23,44]. The electrochemical current in the region of 0.3–0.6 V/NHE is larger for the catalyst supported on MC than for the catalyst supported on Vulcan. It is evident that the high surface area (double layer) and electroactive superficial groups (pseudocapacitance) of the MC produce an enhanced current in this region. At the same time, the OH^- reduction process and adsorption-desorption of hydrogen seems to be hidden on MC.

Fig. 7b (VC) and 7 g (MC) show that the shape of the cyclic voltammetry for the ORR in O_2 saturated solutions, in these figures an enhancement of the electrochemical current is observed due to the oxygen reduction. When 0.5 M methanol is added to the solution (Fig. 7c (VC) and 7 h (MC)) the current-potential behavior is very similar to those without methanol. However, lower current values were observed in solutions containing methanol, which could be attributed to the diffusion competition between methanol and oxygen [63].

Fig. 7d (VC) and 7i (MC) show the ionic current responses, corresponding to carbon dioxide formation when the potential sweep is applied. Fig. 7e (VC) and 7j (MC) show the ionic responses corresponding to methylformiate evolution. Both responses, carbon dioxide and methylformiate formation, do not change over the analyzed potential range, indicating that those species are not formed i.e. the catalyst is methanol tolerant.

Further evidence of the methanol tolerance of the $PdNi_2$/VC catalysts was obtained through chronoamperometry measurements coupled with mass spectrometry. For comparison, a potential jump to a methanol oxidative potential was performed for Pt/VC and $PdNi_2$/VC. Fig. 8 shows the ionic currents evolution for $m/z = 44$, attributed to CO_2, for Pt/

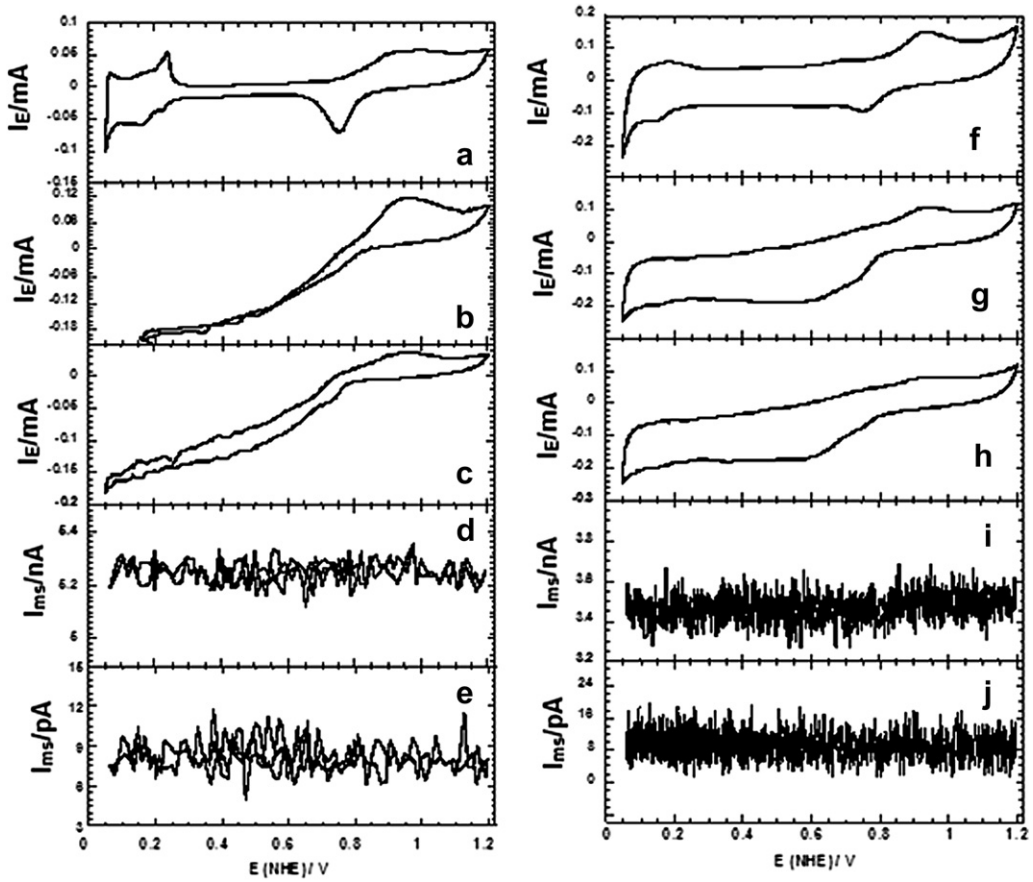

Fig. 7 – Cyclic voltammetry of $PdNi_2$ supported on VC (a–e) and MC (f–j). Current-potential curves in: a,f) 0.5 M H_2SO_4; b,g) O_2 saturated 0.5 M H_2SO_4; c,h) O_2 saturated 0.5 M CH_3OH/0.5 M H_2SO_4. Ionic DEMS current-potential curves in O_2 saturated 0.5 M CH_3OH/0.5 M SO_4H_2 for: d,i) $m/z = 44$ (CO_2); e,j) $m/z = 60$ (methylformiate). Scan rate of 10 m Vs^{-1}, without rotation.

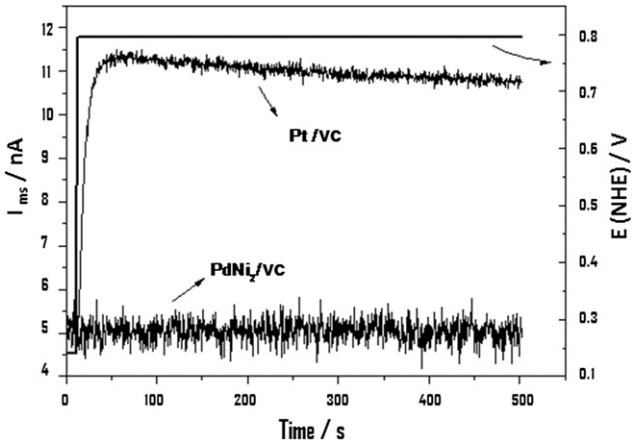

Fig. 8 – Time evolution of the ionic DEMS current corresponding to CO_2 ($m/z = 44$) in 0.5M H_2SO_4 + 0.5M CH_3OH solution for Pt/VC and $PdNi_2$/VC.

VC and $PdNi_2$/VC at 0.8 V. It can be seen that under these conditions, CO_2 is observed as a product of the methanol oxidation for the Pt/VC catalyst, while CO_2 was not detected for the $PdNi_2$ catalyst.

In summary, the DEMS data demonstrate that the $PdNi_2$/C catalyst is almost completely methanol tolerant under the test conditions and meet the conditions required for a suitable cathode material for DMFC.

4. Conclusions

Nanoparticulated $PdNi_2$ catalyst was synthesized by chemical reduction of the corresponding transition metal chlorides with $NaBH_4$ in aqueous media and supported on a novel mesoporous carbon, with a specific area more than double than that of Vulcan carbon.

The morphological and composition characterizations of the $PdNi_2$/MC and $PdNi_2$/VC catalysts seems to indicate a higher degree of Ni alloying and a smaller nanoparticle size for the catalyst supported on MC, probably as a result of its higher specific area and the presence of superficial groups which enhance metal alloying.

The electrochemical characterizations indicate that the $PdNi_2$ catalyst supported on MC exhibits a lower overpotential for the same current density, as compared to that supported on Vulcan. Results of kinetic parameters on the $PdNi_2$/MC catalyst showed that it is able to drive the ORR at very similar rate than Pd- and Pt-based alloys reported in literature as the state of the art, with the advantage of a very low noble metal loading. This could be the result of a best dispersion of the $PdNi_2$ nanoparticles and to the higher amount of Ni alloyed in the $PdNi_2$/MC catalyst.

Finally, DEMS experiments performed for the first time on these catalysts showed that the $PdNi_2$/MC catalyst has no activity for the methanol oxidation in the range 0–1.4 V/NHE.

In summary, our results clearly indicate that the $PdNi_2$/MC catalyst would be a suitable cathodic catalyst for DMFC where a high activity for the ORR, along with a good tolerance for methanol, is required.

Acknowledgments

The authors thank financial support from bilateral project México-Argentina, CONACYT-MINCYT 2008-2010, CONACYT (México) and ANPCyT (Argentina, PICT-PAE 2097). GRS and YRJT thank CONACYT and CONICET, respectively, for doctoral fellowship. HRC and MMB are permanent research fellows of CONICET. The authors thank to M.A. Leyva for assistance in XRD analysis.

Appendix. Supplementary material

Supplementary material associated with this article can be found, in the online version, at doi:10.1016/j.ijhydene.2011.08.113.

REFERENCES

[1] Martínez-Casillas D, Vázquez-Huerta G, Solorza-Feria O. Electrocatalytic reduction of dioxygen on PdCu for PEM fuel cells. J Power Sources 2011;196:4468–74.
[2] Mazumder V, Lee Y, Sun S. Recent development of active nanoparticle catalyst for fuel cell reactions. Adv Funct Mat 2010;20:1224–31.
[3] Li Y, Somorjai GA. Nanoscale advances in catalysis and energy applications. Nanoletters 2010;10:2289–95.
[4] Bonnemann H, Khelashvili G. Efficient fuel cell catalysts emerging from organometallic chemistry. Appl Organomet Chem 2010;24:257–68.
[5] Vielstich W, Gasteiger HA, Lamm A. Handbook of fuel cells: fundamentals, technology and applications. New York: Wiley; 2003.
[6] Salgado JRC, Alcaide F, Álvarez G, Calvillo L, Lázaro MJ, Pastor E. Pt-Ru electrocatalysts supported on ordered mesoporous carbon for direct methanol fuel cell. J Power Sources 2010;195:4022–9.
[7] Salgado JRC, Antolini E, González ER. Carbon supported Pt-Co alloys as methanol-resistant oxygen reduction electrocatalysts for direct methanol fuel cells. Appl Catal B Environ 2005;57:283–90.
[8] Shao M. Palladium-based electrocatalysts for hydrogen oxidation and oxygen reduction reactions. J Power Sources 2011;196:2433–44.
[9] Antolini E. Palladium in fuel cell catalysis. Energy Envir Sci 2009;2:915–31.
[10] Shao M, Sasaki K, Liu P, Adzic R. Pd_3Fe and Pt monolayer-modified Pd_3Fe electrocatalysts for oxygen reduction. Z Phys Chem 2007;221:1175–90.
[11] Kim J, Park JE, Momma T, Osaka T. Synthesis of Pd-Sn nanoparticles by ultrasonic irradiation and their electrocatalytic activity for oxygen reduction. Electrochim Acta 2009;54:3412–8.
[12] Nie M, Shen PK, Wei Z. Nanocrystaline tungsten carbide supported Au-Pd electrocatalyst for oxygen reduction. J Power Sources 2007;167:69–73.
[13] Li B, Prakash J. Oxygen reduction reaction on carbon supported palladium-nickel alloys in alkaline media. Electrochem Commun 2009;11:1162–5.

[14] Savadogo O, Lee K, Oishi K, Mitsushima S, Kamiya N, Ota KI. New palladium alloys catalyst for the oxygen reduction reaction in an acid medium. Electrochem Commun 2004;6:105–9.
[15] Fouda-Onana F, Bah S, Savadogo O. Palladium-copper alloys as catalysts for oxygen reduction reaction in acid media I: correlation between the ORR kinetics parameters and intrinsic properties of the alloys. J Electroanal Chem 2009;636:1–9.
[16] Shao MH, Huang T, Liu P, Zhang J, Sasaki K, Vukmirovic MB, et al. Palladium monolayer and palladium alloy electrocatalysts for oxygen reduction. Langmuir 2006;22:10409–15.
[17] Zhang L, Lee K, Zhang JJ. The effect of heat treatment on nanoparticle size and ORR activity for carbon-supported Pd-Co alloys electrocatalysts. Electrochim Acta 2007;52:3088–94.
[18] Wang W, Zheng D, Du C, Zou Z, Zhang X, Xia B, et al. Carbon supported Pd-Co bimetallic nanoparticles as electrocatalysts for the oxygen reduction reaction. J Power Sources 2007;167:243–9.
[19] Di Noto V, Negro E, Lavina S, Gross S, Pace G. Pd-Co carbon-nitride electrocatalysts for polymer electrolyte fuel cells. Electrochem Acta 2007;53:1604–17.
[20] Wang XP, Kariuki N, Vaughey JT, Goodpaster J, Kumar R, Myers DJ. Bimetallic Pd-Cu oxygen reduction electrocatalysts. J Electrochem Soc 2008;155:B602–9.
[21] Fernandez JL, Raghuveer V, Manthiram A, Bard AJ. Pd-Ti and Pd-Co-Au electrocatalysts as a replacement for platinum for oxygen reduction in proton exchange membrane fuel cells. J Am Chem Soc 2005;127:13100–1.
[22] Zhao J, Sakar A, Manthiram A. Synthesis and characterization of Pd-Ni nanoalloy electrocatalysts for oxygen reduction reaction in fuel cells. Electrochim Acta 2010;55:1756–65.
[23] Ramos-Sánchez G, Solorza-Feria O. Synthesis and characterization of $Pd_{0.5}Ni_xSe_{(0.5-x)}$ electrocatalysts for oxygen reduction reaction in acid media. Int J Hydrogen Energy 2010;35:12105–10.
[24] Lee K, Savadogo O, Ishihara A, Mitsushima S, Kamiya N, Ota K. Methanol-tolerant oxygen reduction electrocatalysts based on Pd-3D transition metal alloys for direct methanol fuel cells. J Electrochem Soc 2006;153:A20–4.
[25] Lopes T, Antolini E, Gonzalez ER. Carbon-supported Pt-Pd alloy as an ethanol tolerant oxygen reduction electrocatalyst for direct ethanol fuel cells. Int J Hydrogen Energy 2008;33:5563–70.
[26] Zhao Y, Yang X, Tian J, Wang F, Zhan L. Methanol electro-oxidation on Ni@Pd core-shell nanoparticles supported on multi-walled carbon nanotubes in alkaline media. Int J Hydrogen Energy 2010;35:3249–57.
[27] Shen SY, Zhao TS, Xu JB, Li YS. Synthesis of PdNi catalysts for the oxidation of ethanol in alkaline direct ethanol fuel cells. J Power Sources 2010;195:1001–6.
[28] An L, Zhao TS, Shen SY, Wu QX, Chen R. Performance of a direct ethylene glycol fuel cell with an anion-exchange membrane. Int J Hydrogen Energy 2010;35:4329–35.
[29] Li YS, Zhao TS. A high-performance integrated electrode for anion-exchange membrane direct ehanol fuel cells. Int J Hydrogen Energy 2011;36:7707–13.
[30] Che G, Lakshmi BB, Fischer ER, Martin CR. Çarbon nanotube membranes for electrochemical energy storage and production. Nature 1998;393:346–9.
[31] Bessel CA, Laubernds K, Rodríguez NM, Baker RTK. Graphite nanofibers as an electrode for fuel cell applications. J Phys Chem B 2001;105:1115–8.
[32] Anderson ML, Stroud RM, Rolison DR. Enhancing the activity of Fuel-cell reactions by designing three-dimensional nanostructured architectures: catalyst-modified carbon-silica composite aerogels. Nano Lett 2002;2:235.
[33] Yu J, Kang S, Yoon SB, Chai G. Fabrication of ordered uniform porous carbon networks and their applications to catalyst supporter. J Am Chem Soc 2002;124:9832–3.
[34] Pacheco-Catalan D, Morales E, Smit M, Acosta JL. Electrocatalytic activity towards oxygen reduction of mesoporous carbon/conducting polymer composites application to PEM fuel cells. J New Mat Electrochem Syst 2009;12:115–8.
[35] Wang G, Sun G, Zhou Z, Liu J, Wang Q, Wang S, et al. Performance improvement in direct methanol fuel cell cathode using high mesoporous area catalyst support. Electrochem Solid State Let 2005;8:A12–6.
[36] Arico AS, Srinivasan S, Antonucci V. DMFCs: from fundamental aspects to technology development. Fuel Cells 2001;1:133–61.
[37] Hou Z, Yi B, Zhang H. Preparing high loading Pt/C by modifying the carbon support. Electrochem Solid-State Lett 2003;6:A232–5.
[38] Bruno MM, Cotella NG, Miras MC, Koch T, Seidler S, Barbero C. Monolithic porous carbon prepared from resorcinol/formaldehyde gels with cationic surfactants. Colloids Surf A 2010;358:13–20.
[39] Bruno MM, Planes GA, Miras MC, Barbero CA, Pastor Tejera E, Rodríguez JL. Synthetic porous carbon as support of platinum nanoparticles for fuel cell electrodes. Mol Crys Liq Crys 2010;521:229–36.
[40] Bruno MM, Franceschini EA, Planes GA, Corti HR. Electrodeposited platinum catalysts over hierarchical carbon monolithic support. J Appl Electrochem 2010;40:257–63.
[41] Bruno MM, Corti HR, Balach J, Cotella GN, Barbero CA. Hierarchical porous materials: capillaries in mesoporous carbon. Funct Mat Lett 2009;2:135–8.
[42] Hutson ND, Yang RT. Theoretical basis of the Dubinin-Rudushkevich isotherm equation. Adsorption 1997;3:189–95.
[43] Rouquerol F, Rouquerol J, Sing K. Adsorption by powders and porous Solids. San Diego: Academic Press; 1999.
[44] Ramos-Sánchez G, Yee-Madeira H, Solorza-Feria O. PdNi Electrocatalyst for oxygen reduction in acid media. Int J Hydrogen Energy 2008;33:3596–600.
[45] Planes G, Garcia G, Pastor E. High performance mesoporous Pt electrode for methanol electrooxidation. A DEMS study. Electrochem Commun 2007;9:839–44.
[46] Guo Y, Usman Azmat M, Liu X, Ren J, Wang Y, Lu G. Controllable synthesis of hexagonal close-packed nickel nanoparticles under high nickel concentration and its catalytic properties. J Mater Sci 2011;46:4606–13.
[47] Malheiro AR, Perez J, Villulas HM. Well-Alloyed PtFe/C nanocatalysts of controlled composition and same particle size: oxygen reduction and methanol tolerance. J Electrochem Soc 2009;156:B51–8.
[48] Qu Z, Geng H, Wang X, Zhao C, Ji H, Zhang C, et al. Novel nanocrystalline PdNi alloy catalyst for methanol and ethanol electro-oxidation in alkaline media. J Power Sources 2011;196:5823–8.
[49] Bagmut AG, Shipkova IG, Zhuchkov VA. Formation, structure and magnetic changes at annealing of films deposited by laser sputtering of Ni and Pd. J Surf Invest X-Ray syncr Neutron Tech 2011;5:460–4.
[50] Sotelo-Mazón P, González-Huerta RG, Cabañas-Moreno JG, Solorza-Feria O. Mechanically milled Ru_xFe_y electrocatalysts for oxygen reduction in acid media. Int J Electrochem Sci 2007;2:523–33.
[51] Suárez-Alcántara K, Rodríguez-Castellanos A, Dante R, Solorza-Feria O. $Ru_xCr_ySe_z$ electrocatalyst for oxygen reduction in a polymer electrolyte membrane fuel cell. J Power Sources 2006;157:114–20.

[52] Bard AJ, Faulkner L. Electrochemical methods: principles and applications. New York: Wiley; 2001. 341.
[53] Salvador-Pascual JJ, Citalán-Cigarroa S, Solorza-Feria O. Kinetics of oxygen reduction reaction on nanosized Pd electrocatalyst in acid media. J Power Sources 2007;172: 229–34.
[54] Xiong L, Kannan AM, Manthiram A. Pt-M (M=Fe, Co, Ni and Cu) electrocatalysts synthesized by an aqueous route for proton exchange membrane fuel cells. Electrochem Commun 2002;4:898–903.
[55] Kariuki NN, Xiaoping W, Mawdsley JR, Ferrandon MS, Niyogi SG, Vaughey JT, et al. Colloidal synthesis and characterization of carbon-supported Pd-Cu nanoparticle oxygen reduction electrocatalyst. Chem Mater 2010;22: 4144–52.
[56] Wang R, Li H, Ji S, Wang H, Lei Z. Pt decorating of PdNi/C as electrocatalysts for oxygen reduction. Electrochim Acta 2010; 55:1519–22.
[57] Mustain WE, Kepler K, Prakash J. Investigations of carbon-supported $CoPd_3$ catalysts as oxygen cathodes in PEM fuel cells. Electrochem Commun 2006;8:406–10.
[58] Sarkar A, Murugan AV, Manthiram A. Low cost Pd–W nanoalloy electrocatalysts for oxygen reduction reaction in fuel cells. J Mater Chem 2009;19:159–65.
[59] Jusys Z, Behm RJ. Methanol oxidation on a carbon-supported Pt fuel cell catalyst. A kinetic and mechanistic study by differential electrochemical mass spectrometry. J Phys Chem B 2001;105:10874–83.
[60] Jusys Z, Behm RJ. Simultaneous oxygen reduction and methanol oxidation on a carbon-supported Pt catalyst and mixed potential formation-revisited. Electrochim Acta 2004; 49:3891–900.
[61] Jusys Z, Kaiser J, Behm RJ. Methanol electrooxidation over Pt/C fuel cell catalysts: dependence of product yields on catalyst loading. Langmuir 2003;19:6759–69.
[62] Colmenares L, Jusys Z, Behm RJ. Activity, selectivity, and methanol tolerance of Se-modified Ru/C cathode catalysts. J Phys Chem C 2007;111:1273–83.
[63] Maillard F, Martin M, Gloaguen F, Léger JM. Oxygen electroreduction on carbon-supported platinum catalysts. Particle-size effect on the tolerance to methanol competition. Electrochim Acta 2010;47:3431–40.